MNE 14 (2022) 100115

Contents lists available at ScienceDirect

Micro and Nano Engineering

journal homepage: www.sciencedirect.com/journal/micro-and-nano-engineering

# Sapphire nanophotonics: Fabrication challenges and optical properties

Yi-An Chen, Kun-Chieh Chien, I-Te Chen, Chih-Hao Chang *

*Walker Department of Mechanical Engineering University of Texas at Austin, Austin, TX 78712, USA*

A R T I C L E I N F O

*Keywords:*
Sapphire nanostructures
Nanophotonics
Reactive ion etching
Pattern transfer
Nanofabrication

A B S T R A C T

Sapphire has many optical applications in nanophotonics and optoelectronic devices due to its high index, broadband transparency, and chemical and physical stability. However, sapphire is notoriously difficult to process, cut, and micromachine. As a result, patterning high density and aspect ratio nanostructures in sapphire, such as those needed for nanophotonics, are challenging. Here, we demonstrate an effective fabrication approach to pattern high aspect-ratio sapphire nanostructures using a multilayer etching process. This approach is based on the concept of designing the etching selectivities of neighboring masks to significantly increase the overall etch selectivity. Using polymer nanostructures with initial height of 50 nm, the process is used to demonstrate antireflection sapphire nanostructures with feature width of 170 nm and depth of 345 nm, resulting in aspect ratio of 2.03. The optical properties of the sapphire nanostructures have been characterized and the surface reflectivity is reduced from 6% to 2% at near normal incidence and from 39% to 11% at 70° incident angle. The experimental data also indicates that the antireflection effect operates at broadband wavelength from 350 to 1000 nm. This work demonstrate that sapphire nanostructures can be patterned by using multiple masks to achieve etch selectivity over 7, and can find applications in sapphire-based nanophotonics, metasurfaces, and optoelectronics devices.

## 1. Introduction

Transparent substrates have many optical applications such as windows, lenses, nanophotonic structures, metasurfaces, solid-state lighting, and optoelectronic devices [1–8]. Most existing transparent substrates are based on silica, which has established manufacturing processes. Silicon oxide and silica-based glass are also relatively easy to micromachine and the subtractive etching processes are well understood. However, there are several limitations with silica-based glass. First, silica has relatively low index of around 1.45, which offers a limited index contrast and phase delay for nanophotonic elements and metasurfaces. Second, silica can have absorption peaks in the IR and has limited transmission for wavelength longer than 3.5 μm, limiting their application for visible to NIR range. Lastly, silica-based glass also lacks mechanical and thermal durability and is subjected to scratch damage and low operating temperature. These properties limit the application of silica-based glass in extreme environments.

In contrast with silica, sapphire and other alumina-based transparent ceramics including aluminum oxynitride (AlON), yttrium aluminum garnet (YAG), and magnesium aluminate spinel ($MgAl_2O_4$) have a number of key advantages due to their chemical and physical stabilities [9,10]. With Mohs hardness scale of 9, sapphire is among the hardest of all naturally occurring material only behind diamond, and is ideal as a protective material for wear and scratch resistance. Sapphire also has high Young's modulus of 350 GPa and compressive and tensile strengths of 2 and 0.5 GPa, respectively. In addition, sapphire has extremely broad optical transmission from wavelength of 0.25 to 5 μm, which is critical for infrared (IR) optics. It also has high optical refractive index in the range of 1.75 in the visible and can increase light trapping and reduce losses in integrated photonics. Sapphire is also a good thermal conductor with 40 W/mK and has high melting point of 2030 °C, making it ideal for high-temperature applications. Furthermore, it is chemically inert and is resistant to corrosion. These properties make sapphire attractive for long-term protection in extreme environments such as high temperature, pressure, and mechanical loading. To date, one of the most common applications for sapphire in defense is missile domes [9], which requires the material to survive through harsh launch conditions as well as high light transmission in the IR for various optical signals.

Sapphire also has broad applications in nanophotonic and optoelectronic devices due to its optical and high temperature stability [2,3,5,6]. In comparison to silica-based photonics, which has absorption peaks in the near infrared (NIR), sapphire photonics can maintain high

* Corresponding author.
*E-mail address:* chichang@utexas.edu (C.-H. Chang).

https://doi.org/10.1016/j.mne.2022.100115
Received 30 December 2021; Received in revised form 28 January 2022; Accepted 21 February 2022
Available online 24 February 2022

NIR transmission up to 5 μm. Recent work using silicon-on-sapphire integrated waveguides have demonstrated operation in the NIR region up to 4.5 μm wavelength [11,12]. In addition, sapphire photonics can operate at much higher temperature when compared with silica. One example is sapphire fiber Bragg grating for measuring strain and temperature measurement, which can operate from room temperature to elevated temperature of 1400 °C [13,14]. Sapphire-based white-light interferometric fiber sensor have also demonstrated high operation temperature of 1600 °C [15]. Sapphire substrates are also attractive for epitaxial growth of III-V semiconductors and have applications in UV LEDs and laser diodes [16–19]. The benefits of fabricating photonic devices on sapphire materials includes higher index, broader operation range in the IR, and higher operation temperature, which can lead to broader applications for photonics in extreme environments.

However, one significant challenge is that creating photonic nanostructures in sapphire and other alumina-based materials is extremely difficult. This can be attributed to their chemical inertness, which results in low etch rates during plasma etching and other traditional micromachining processes where reaction chemistry plays a key role [23–40]. Wet etching of sapphire in high-temperature acid solutions (such as $H_2SO_4$, $H_3PO_4$, etc.) is one method to pattern surface microstructures [20–26]. However, given the wet etching approach such structures have low feature resolution and are typically limited to the 10 μm scale. The etch depth are also difficult to precisely control and are relatively shallow, resulting in low aspect ratio less than 1. Furthermore, the etch isotropy and anisotropy in wet etching is constraint by the crystal structure of the material and cannot be well controlled. Previous work have also demonstrated reactive ion etching (RIE) of sapphire microstructures [27–34]. However, these structures generally have large features in the ~10 μm range. Finer sub-micrometer structures [1,3] have also been demonstrated, but the structures have random order and high feature roughness. Recent work using nanoimprint have successfully demonstrated periodic nanostructures in sapphire [29]. However, the etch depth is relatively low due to the low etch selectivity, resulting in low aspect ratio nanostructures. Therefore, fabricating high resolution sapphire nanostructures with high selectivity for high-efficiency photonic and optoelectronics is still a critical challenge.

In this work, we demonstrate an effective method to pattern high aspect-ratio nanostructures in sapphire substrates. The proposed method utilizes multiple masking materials to overcome the inherently low etch selectivity of sapphire during RIE. By selecting neighboring masks with high selectivity, a relatively short polymer features can be pattern transferred deep into the sapphire substrate and achieve high overall etch selectivity. The advantage of this approach is that is compatible with existing pattern transfer processes and can be readily integrated with existing infrastructure. To demonstrate the proposed concept, the process is used to fabricate antireflection moth-eye sapphire nanostructures with aspect ratio of 2. The fabricated sapphire nanostructures can effectively suppress the Fresnel losses over broadband wavelength band and wide incident angles. This work demonstrates that high-resolution, periodic sapphire nanostructures can be fabricated with high etch selectivity, which can open the door to sapphire photonics and optoelectronics.

## 2. Technical approach

The multilayer mask etching processes schematic to pattern high aspect-ratio sapphire nanostructures is shown in Fig. 1. The goal is to use a multiple stack consisting of silicon oxide, polycrystalline silicon, and sapphire since the etch rates of these materials greatly differ in F, Cl, and Br-based RIE, to transfer a relatively short polymer structures into the underlying sapphire substrate. Initially, a sapphire substrate with (0001) orientation is deposited with 430 nm silicon nitride and 350 nm poly-silicon using low-pressure chemical vapor deposition (LPCVD). Then, 100 nm of $SiO_2$ layer is deposited using electron beam evaporation. Polystyrene (PS) nanospheres with 200 nm diameter are then assembled on the stack to form a close-packed hexagonal nanostructure array. The PS nanospheres are then etched in oxygen plasma etching (PE) to reduce the diameters to 50 nm to reduce the duty cycle of the structure. Since the PE process is isotropic, the etched thickness of the PS mask is also around 50 nm and is relatively thin. Note other patterning techniques such as interference lithography or nanoimprint lithography can also be used to pattern the initial features to create periodic patterns. In prior work we have used multilayer masks with fewer layers to demonstrate improved etching into sapphire, however the features are larger and the etch chemistry not optimized. Therefore the results yield structures with low aspect ratio (0.5) and limited AR effects [35].

The fabrication results and the evolution of the multilayer mask through the etching process is shown in Fig. 2. The top-view SEM of PS nanospheres after 1 min 24 s of $O_2$ PE trimming process (pressure 700 mTorr, RF power 300 W, and ICP power 100 W) is shown in Fig. 2(a). The structures are in a non-close-packed hexagonal array with diameter around 100 nm, which is further reduced to 50 nm by additional etching. As noted previously, the neighboring layers of the multilayer masks are selected to enhance the overall etch selectivity versus sapphire. The PS pattern is used as a mask to etch into $SiO_2$ with etching selectivity $\alpha_{SiO2} = 2.1$ using $CHF_3$ RIE (6 min etch time, RF power 150 W, pressure 20 mTorr, flow rate 20 sccm). The $SiO_2$ structure is an effective mask to etch poly-Si with etching selectivity $\alpha_{Si} = 2.9$ using HBr RIE (3.5 min etch time, RF power 250 W, ICP power 200 W, pressure 8 mTorr, flow rate 30 sccm). The resulting nanostructures in the poly-Si layer can be seen in the cross-section SEM image shown in Fig. 2(b), which has the same period as the PS structure but has a much taller height of 450 nm. The poly-Si structures then serve as an effective mask to etch the underly nitride, which has an etching selectivity $\alpha_{SiN} = 2.0$ using $CHF_3$ mixed with $O_2$ (24 min etch time, RF power 250 W, pressure 15 mTorr, $CHF_3$ flow rate 25 sccm, $O_2$ flow rate 5 sccm). $O_2$ was added in the etching process to mitigate the polymer redeposition process, which negatively impacts the pattern transfer by increasing the duty cycle of the nanostructures in the silicon nitride layer. The final remaining multilayer etching mask includes poly-Si and nitride has a thickness of 500 nm and is shown in Fig. 2(c), which can serve as a thick mask for pattern transfer into the underlying substrate. The etching selectivity of sapphire vs nitride using $BCl_3$ ICP-RIE (9 min 43 s etch time, RF power 300 W, ICP power 1500 W, pressure 8 mTorr, flow rate 30 sccm) is around $\alpha_{sapphire} = 0.6$, therefore the structure height decreases when etching into sapphire. By designing the etch selectivies of the multilayer,

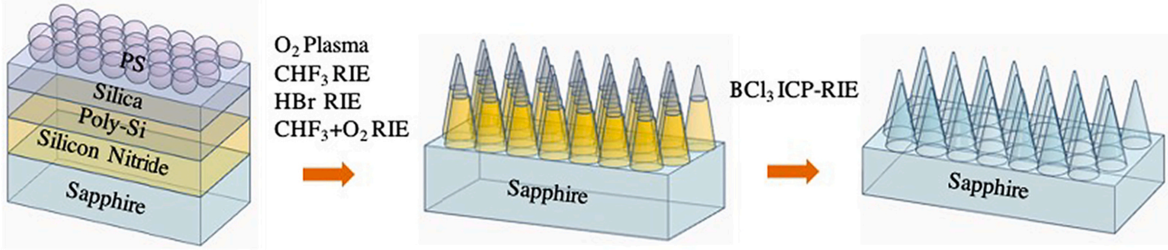


**Fig. 1.** Schematic of multilayer etching mask processes to pattern higher aspect-ratio sapphire nanostructures.

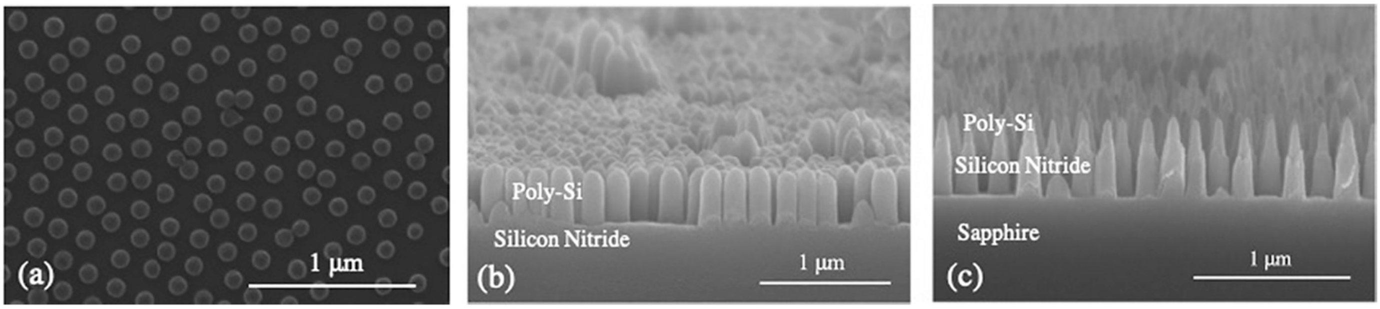


**Fig. 2.** SEM images of the multilayer etch masks. (a) Non-close-packed hexagonal array of PS nanospheres after $O_2$ plasma etching process, (b) pattern transferred nanostructures in poly-Si mask layer, and (c) final mask consisting of poly-Si and silicon nitride.

the total etch selectivity can be calculated as $\alpha_{total} = \alpha_{SiO2}\alpha_{Si}\alpha_{SiN}\alpha_{sapphire} = 7.3$, indicating that 50 nm thick polystyrene mask can lead to 365 nm tall sapphire nanostructures.

The cross-section SEM images of the fabricated sapphire nanostructures after cleaning the samples in 49% HF to remove any residual masking materials are shown in Fig. 3. Here the sapphire nanostructures follow a graduate tapered profile and have 170 nm width and 345 nm height, resulting in an aspect-ratio of 2.03. It can be observed that the structures have uniform feature geometry and are locally periodic. Note the sapphire pillars has a slight taper near the top, which is due to the high etch rate and shrinking of the nitride mask near the end of the $BCl_3$ etch step. A number of defects can be observed, which is characteristics of the PS colloidal self-assembly process. In this mask design, 50 nm thick PS mask with 200 period is able to pattern sapphire nanostructures with around 345 nm height, an improvement by a factor of 6.9. Note that if a taller polymer structure is used, the thickness of the multilayer masks can be increased to achieve greater etch depth into the sapphire substrate and further improve the structure aspect ratio. This process overcomes the key limitation in patterning nanostructures in sapphire substrates, which is that etching selectively into sapphire is well below 1. The results demonstrate that by designing the material and etch chemistry at each mask layer, the combined total etching selectivity can be greatly increased to around 7.

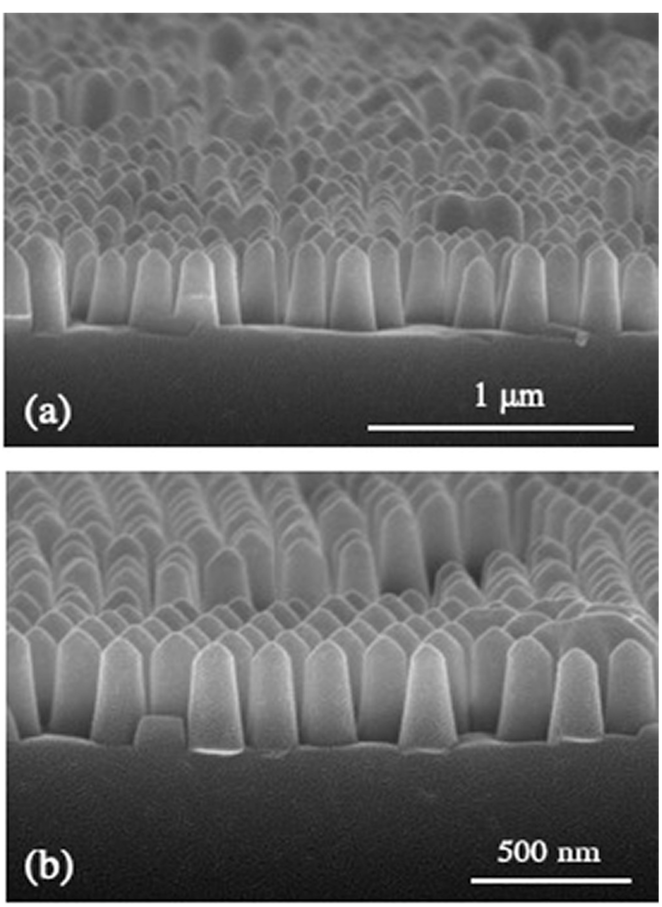


**Fig. 3.** SEM image of fabricated higher aspect-ratio sapphire nanostructures under (a) lower magnification and (b) higher magnification.

## 3. Optical characteristic and discussion

The optical properties of the fabricated sapphire nanostructures are characterized to demonstrate their antireflection properties. The surface reflectivity is measured using a 633 nm HeNe laser (Model 30,995, Research Electro-Optics, Inc.) as a function of incident angles from 0° to 70° with 1° resolution for both transverse electric (TE) and transverse magnetic (TM) polarizations. A photodiode detector (Model 918D-UV-OD3, Newport Co.) is used to measure the light reflection intensity. The measured reflectivity is compared with theoretical prediction, which is modeled using Fresnel equation for the planar sapphire sample and rigorous coupled-wave analysis (RCWA) for the nanostructured samples. The RCWA simulation models the antireflection structures as discrete slices with air ($n = 1$) and sapphire ($n = 1.75$) periodic index modulation along both $x$ and $y$ directions in a square lattice with 200 nm period. The 2D nanostructure profile is obtained from SEM image and approximated by varying the duty-cycle between 0.175 and 0.85.

The measured reflectivity of the fabricated sapphire antireflection nanostructures under TE and TM mode is plotted in Fig. 4 (a) and (b), respectively. It can be observed that the data matches well with the theoretical models. In the measurement, the reflectivity under TE mode is reduced from 6% to 2% near normal incidence for the sapphire substrate with the nanostructures. Note the reflectivity of the planar sapphire substrate is higher than that of silica-based glass due to higher refractive index. The reflectivity can be further suppressed from 39% to 11% at 70° incident angle. The experiment and simulation data under TE mode indicate that the antireflection effect is more dramatic when the incident angle is increased since the reflection losses are higher. The reflectivity under TM mode is reduced from 8.5% to 3% near normal incidence for the sapphire substrate with nanostructures. However, the reflectivity of the nanostructured sample is similar to the planar sample at around 60° incident angle in TM mode. This can be attributed to the Brewster angle effect, where the transmission for the planar sample is 100%. The error bar for the measurement is around 0.1%, which is the standard deviation of measurements data. These results demonstrate that sapphire nanostructures with higher aspect-ratio are effective in mitigating surface reflection losses due to Fresnel reflection and the effects are more dramatic at higher incident angle.

The broadband antireflection effects of the fabricated sapphire nanostructures are also studied using a spectrometer (HR4Pro, Ocean Insight.). The broadband reflectivity of the sapphire nanostructured sample at 5° and 45° incidence angles are plotted in Fig. 5 (a) and (b),

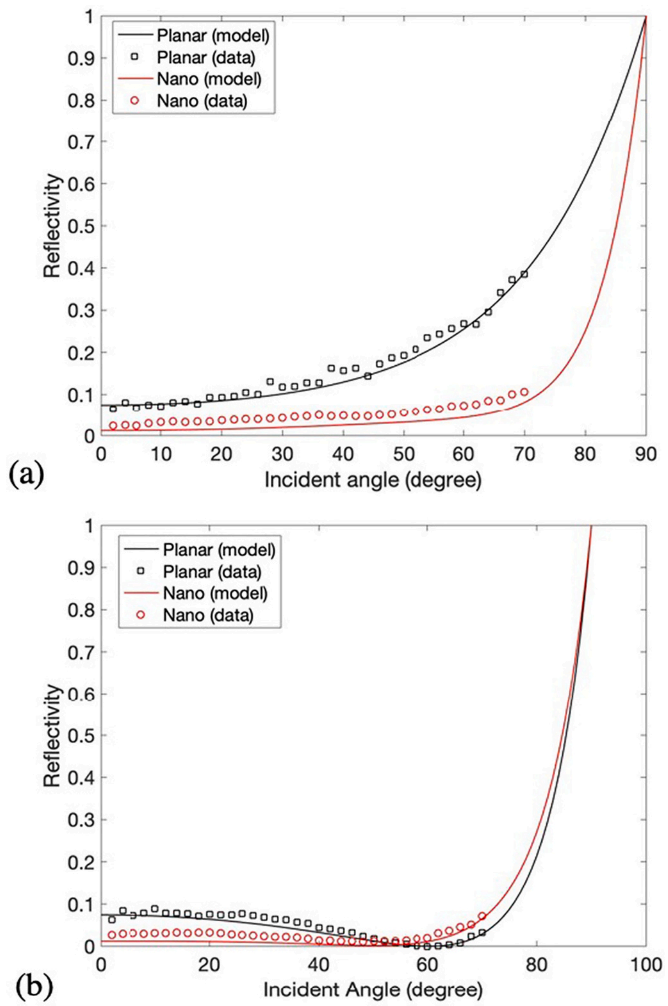


**Fig. 4.** Experimentally measured and simulated reflectivity data of planar and antireflection sapphire nanostructure samples under (a) TE and (b) TM-polarized light with 633 nm wavelength. The measurement uncertainty is around 0.1%.

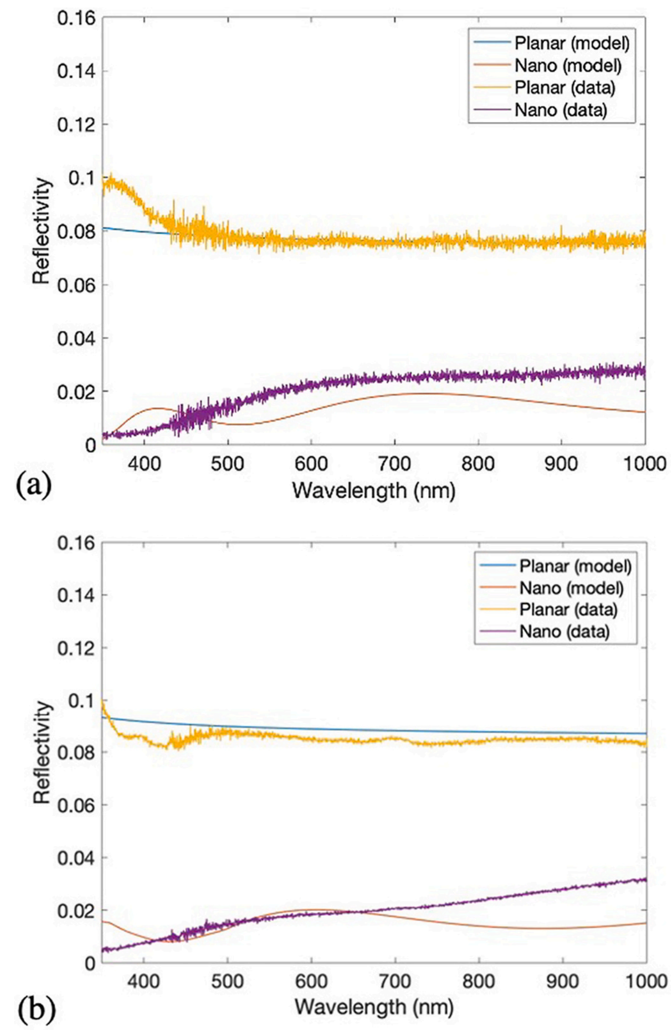


**Fig. 5.** Broadband measured and modeled reflectivity data at (a) 5 degree and (b) 45 degree incidence angle for sapphire substrate with and without surface nanostructures.

respectively. The simulation data of planar and nanostructured sample are obtained using Fresnel equations and RCWA, taken into account the material dispersion. From the experimental results, the reflectivity is reduced from 9.2% to 0.3% at 5° incidence angle for the sapphire substrate with nanostructures at 350 nm wavelength. At 1000 nm wavelength, the reflectivity is reduced from 7.6% to 2.6% at 5° incidence angle with employing nanostructures on sapphire substrate. The reduced antireflection effect can be attributed to the relatively short nanostructures compared to the wavelength. At higher incident angle of 45°, the reflectivity can be reduced from 9.7% to 0.4% at 350 nm wavelength for the sapphire substrates with the nanostructures. At 45° and 1000 nm wavelength, the reflectivity of nanostructured sapphire sample is reduced from 8.2% to 3.1% comparing to planar sapphire sample. Some signal noise can be seen at the longer wavelength region. However, it can be observed that the reflectivity is reduced by around 6% over broadband when nanostructures are applied. While the experimental data generally agree well with the simulation data, there are some mismatch. This can be attributed to the fabrication yield of the nanostructures and assembly defects during fabrication process. These data indicated that the sapphire nanostructures can have effective antireflection effects over broad wavelength band.

This work demonstrates sapphire nanostructures with etch depth of 345 nm using 50 nm thick PS mask, which is almost a 7-fold improvement. Future work will focus on optimize the thicknesses of the initial polymer structure and the multilayer masks to increase the nanostructures etching depth, which can further increase etch depth and structure aspect ratio. We will also explore the minimum feature sizes that the multilayer etching process can achieve. In addition, the optical properties and antireflection effects using periodic nanostructures will be examined, which can be achieved using more precise lithographic techniques such as laser interference lithography. This can reduce optical scattering, eliminate reflection, and increase transmission of the sapphire nanostructures.

## 4. Conclusion

This work demonstrates a multilayer etch process to pattern nanostructures with increased aspect ratio in sapphire substrates. The proposed approach uses high etching selectivity of neighboring masking layers to overcome the traditional low etch rate of less than 1 observed in sapphire. The result demonstrates that by using a multilayer mask consisting of polymer, $SiO_2$, poly-Si, and silicon nitride, an overall etch selectivity over 7 can be achieved. Using this process, a 50 nm-thick PS structure was pattern transferred into 345 nm of sapphire, an improvement of 6.9 in feature height. The fabricated sapphire nanostructure has aspect ratio of 2.03, which is among the highest reported in the literature for sapphire nanostructures. The fabricated sapphire nanostructures also demonstrated effective broadband and wide-angle antireflection properties. This process lowers the barrier to creating high resolution and aspect ratio structures in sapphire and can pave the way for sapphire-based nanophotonics, metasurfaces, and other optoelectronic devices.

## 5. Methods

The multilayer etch mask is fabricated by depositing 430 nm silicon nitride and 350 nm poly-silicon using LPCVD and 100 nm of SiO2 using electron beam evaporator on (0001) orientation sapphire substrate. PS nanospheres with 200 nm diameter are then assembled on the stack and etched using $O_2$ PE to trim the PS nanosphere (1 min 24 s etch time, pressure 700 mTorr, RF power 300 W, and ICP power 100 W). $CHF_3$ RIE (6 min etch time, RF power 150 W, pressure 20 mTorr, flow rate 20 sccm), HBr RIE (3.5 min etch time, RF power 250 W, ICP power 200 W, pressure 8 mTorr, flow rate 30 sccm), $CHF_3$ mixed with $O_2$ RIE (24 min etch time, RF power 250 W, pressure 15 mTorr, $CHF_3$ flow rate 25 sccm, $O_2$ flow rate 5 sccm) were used to transfer the pattern into the silica, poly-si, and silicon nitride layers, respectively. Then, $BCl_3$ ICP-RIE (9 min 43 s etch time, RF power 300 W, ICP power 1500 W, pressure 8 mTorr, flow rate 30 sccm) is used to transer the pattern into the sapphire substrate. The sapphire sample was dipped into 49% HF for 5 mins and following with 5 mins DI-water rising to remove any remaining mask on the surface before measurement.

## Funding

This work was supported by Army Research Office (ARO) under Grant No. W911NF-17-1-0591 and partially supported by National Science Foundation (NSF) under Grant No. CMMI#1552424.

## Data availability

Data underlying the results presented in this paper are not publicly available at this time but may be obtained from the authors upon reasonable request.

## Declaration of Competing Interest

The authors declare no conflicts of interest.

## Acknowledgments

This work was performed at Texas Materials Institute (TMI), the Nanomanufacturing System for mobile Computing and Energy Technologies (NASCENT), and Texas Nanofabrication Facilities at the University of Texas at Austin, which is supported by the National Science Foundation as part of the National Nanotechnology Coordinated Infrastructure (NNCI) grant NNCI-2025227. This work was supported by Army Research Office (ARO) under Grant No. W911NF-17-1-0591 and partially supported by National Science Foundation (NSF) under Grant No. CMMI#1552424.

## References

[1] Y.-S. Lin, W.-C. Hsu, K.-C. Huang, J.A. Yeh, Appl. Surf. Sci. 258 (2011) 2.
[2] K.-C. Park, H.J. Choi, C.-H. Chang, R.E. Cohen, G.H. McKinley, G. Barbastathis, ACS Nano 6 (2012) 3789.
[3] J.W. Leem, J.S. Yu, Opt. Expr. OE 20 (2012) 26160.
[4] X. Ye, X. Jiang, J. Huang, F. Geng, L. Sun, X. Zu, W. Wu, W. Zheng, Sci. Rep. 5 (2015) 13023.
[5] X.A. Zhang, Y.-A. Chen, A. Bagal, C.-H. Chang, Opt. Lett., OL 42 (2017) 4123.
[6] Y.-A. Chen, S.V. Naidu, Z. Luo, C.-H. Chang, J. Appl. Phys. 126 (2019), 063101.
[7] P. Lalanne, G.M. Morris, Nanotechnology 8 (1997) 53.
[8] Y. Kanamori, M. Sasaki, K. Hane, Opt. Lett., OL 24 (1999) 1422.
[9] L.M. Goldman, R. Twedt, S. Balasubramanian, S. Sastri, In Window and Dome Technologies and Materials XII (International Society for Optics and Photonics) 8016, 2011, p. 801608.
[10] C.T. Warner, T.M. Hartnett, D. Fisher, W. Sunne, in Window and Dome Technologies and Materials IX (International Society for Optics and Photonics) 5786, 2005, pp. 95–111.
[11] Silicon-on-sapphire integrated waveguides for the mid-infrared. https://www.osapublishing.org/oe/fulltext.cfm?uri=oe-18-12-12127&id=199713.
[12] Z. Cheng, X. Chen, C.Y. Wong, K. Xu, C.K.Y. Fung, Y.M. Chen, H.K. Tsang, IEEE Photon. J. 4 (2012) 104.
[13] S.J. Mihailov, D. Grobnic, C.W. Smelser, Opt. Lett., OL 35 (2010) 2810.
[14] S. Yang, D. Homa, G. Pickrell, A. Wang, Opt. Lett., OL 43 (2018) 62.
[15] Y. Zhu, Z. Huang, F. Shen, A. Wang, Opt. Lett., OL 30 (2005) 711.
[16] S. Nakamura, T. Mukai, M. Senoh, Appl. Phys. Lett. 64 (1994) 1687.
[17] H. Hu, B. Tang, H. Wan, H. Sun, S. Zhou, J. Dai, C. Chen, S. Liu, L.J. Guo, Nano Energy 69 (2020), 104427.
[18] M. Shan, Y. Zhang, T.B. Tran, J. Jiang, H. Long, Z. Zheng, A. Wang, W. Guo, J. Ye, C. Chen, J. Dai, X. Li, ACS Photon. 6 (2019) 2387.
[19] T.B. Tran, F. AlQatari, Q.-H. Luc, Sci. Rep. 11 (2021) 4981.
[20] Y.-C. Chen, F.-C. Hsiao, B.-W. Lin, B.-M. Wang, Y.S. Wu, W.-C. Hsu, J. Electrochem. Soc. 159 (2012) D362.
[21] C.-C. Chen, F.C. Hsiao, B.-W. Lin, W.-C. Hsu, Y.S. Wu, ECS J. Solid State Sci. Technol. 2 (2013) R169.
[22] N. Aota, H. Aida, Y. Kimura, Y. Kawamata, M. Uneda, ECS J. Solid State Sci. Technol. 3 (2014) N69.
[23] Y.-C. Chen, B.-W. Lin, W.-C. Hsu, Y.S. Wu, Mater. Lett. 118 (2014) 72.
[24] J. Shen, D. Zhang, Y. Wang, Y. Gan, ECS J. Solid State Sci. Technol. 6 (2017) R24.
[25] J. Shen, D. Zhang, Y. Wang, Y. Gan, ECS J. Solid State Sci. Technol. 6 (2017) R122.
[26] J. Shen, D. Zhang, Y. Wang, Y. Gan, ECS J. Solid State Sci. Technol. 6 (2017) R163.
[27] Etch Characteristics of Al2O3 in ICP and MERIE Plasma Etchers - IOPscience. https://iopscience.iop.org/article/10.1149/1.1865912/pdf.
[28] S.-M. Koo, D.-P. Kim, K.-T. Kim, C.-I. Kim, Mater. Sci. Eng. B 118 (2005) 201.
[29] H. Chen, Q. Zhang, S.Y. Chou, Nanotechnology 26 (2015), 085302.
[30] N. Heiman, V. Minkiewicz, B. Chapman, J. Vac. Sci. Technol. 17 (1980) 731.
[31] C.H. Jeong, D.W. Kim, H.Y. Lee, H.S. Kim, Y.J. Sung, G.Y. Yeom, Surf. Coat. Technol. 171 (2003) 280.
[32] C.H. Jeong, D.W. Kim, J.W. Bae, Y.J. Sung, J.S. Kwak, Y.J. Park, G.Y. Yeom, Mater. Sci. Eng. B 93 (2002) 60.
[33] J.D.B. Bradley, F. Ay, K. Wörhoff, M. Pollnau, Appl. Phys. B Lasers Opt. 89 (2007) 311.
[34] S.-H. Park, H. Jeon, Y.-J. Sung, G.-Y. Yeom, Appl. Opt. AO 40 (2001) 3698.
[35] Y.-A. Chen, I.-T. Chen, C.-H. Chang, J. Vac. Sci. Technol. B 37 (2019), 061606.